

Exploring fractality of microcrystalline diamond films

Cite as: AIP Advances **8**, 075024 (2018); <https://doi.org/10.1063/1.5034469>

Submitted: 11 April 2018 • Accepted: 07 July 2018 • Published Online: 26 July 2018

Vojislav V. Mitic, Hans-Jörg Fecht, Markus Mohr, et al.



View Online



Export Citation



CrossMark

ARTICLES YOU MAY BE INTERESTED IN

Microcrystalline, nanocrystalline, and ultrananocrystalline diamond chemical vapor deposition: Experiment and modeling of the factors controlling growth rate, nucleation, and crystal size

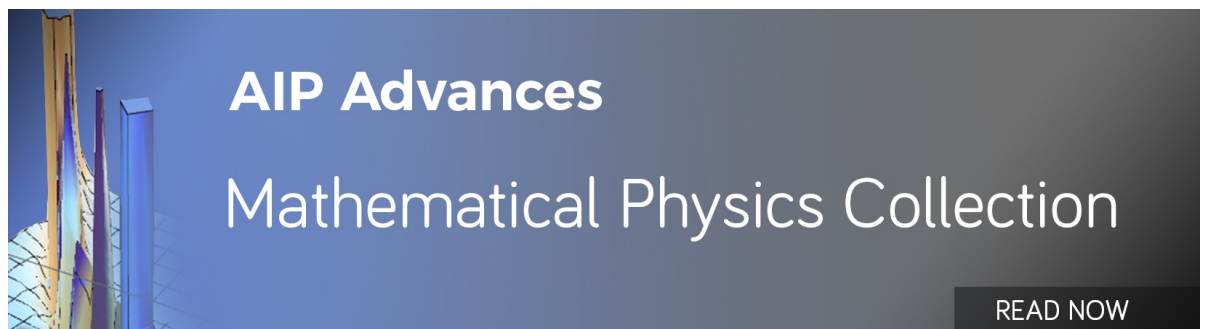
Journal of Applied Physics **101**, 053115 (2007); <https://doi.org/10.1063/1.2696363>

Effective thermal and mechanical properties of polycrystalline diamond films

Journal of Applied Physics **123**, 165105 (2018); <https://doi.org/10.1063/1.5016919>

Anisotropic and inhomogeneous thermal conduction in suspended thin-film polycrystalline diamond

Journal of Applied Physics **119**, 175103 (2016); <https://doi.org/10.1063/1.4948335>



AIP Advances
Mathematical Physics Collection

READ NOW

Exploring fractality of microcrystalline diamond films

Vojislav V. Mitic,^{1,2} Hans-Jörg Fecht,³ Markus Mohr,^{3,a} Goran Lazovic,⁴ and Ljubisa Kocic²

¹*Institute of Technical Sciences of SASA, 11000 Belgrade, Serbia*

²*University of Nis, Faculty of Electronic Engineering, 18000 Nis, Serbia*

³*Institute of Functional Nanosystems, University of Ulm, 89081 Ulm, Germany*

⁴*University of Belgrade, Faculty of Mechanical Engineering, 11120 Belgrade, Serbia*

(Received 11 April 2018; accepted 7 July 2018; published online 26 July 2018)

Diamond is renowned as a material with superlative physical qualities, most of which originate from the strong covalent bonding between its atoms. The possibility to deposit polycrystalline diamond films via chemical vapor deposition (CVD) methods on large areas and on a large variety of substrates is posing numerous scientific challenges but also enables relevant industrial applications. Especially for small grain sizes, the grain's misorientation and consequently the atomic structure of grain boundaries plays a significant role on transport properties and mechanical properties. Hence, the size and shape of the crystallites of poly- and nanocrystalline diamond films are one important key to optimize film properties for their specific applications. Fractal theory helps to find and define order in systems where disorder seems to prevail. Therefore, we apply fractal geometry analysis to characterize the grain morphology and surface topology of CVD grown diamond films. © 2018 Author(s). All article content, except where otherwise noted, is licensed under a Creative Commons Attribution (CC BY) license (<http://creativecommons.org/licenses/by/4.0/>). <https://doi.org/10.1063/1.5034469>

I. INTRODUCTION

Advanced chemical vapor deposition methods, such as the hot filament chemical vapor deposition have made it possible to nucleate and grow homogeneous diamond films composed of small crystallites in the micro- or nanoscale continuously on large areas. Such diamond thin films, with grain sizes down to the nanometer scale, can still preserve most superlative physical qualities that the diamond structure offers¹⁻³ but at the same time exhibit superior mechanical and electrical properties. Thus, new functionalities are being developed in small grained diamond thin films, such as a substantial and variable electrical conductivity⁴⁻⁶ which also exhibits a piezo-resistive effect^{7,8} useful for a number of sensor applications.

Thus, these properties can be tuned and the diamond films can be geometrically tailored to make diamond attractive for high-tech applications, such as micro-mechanical systems, micro-electro-mechanic sensors, anti-wear coatings, optical windows and electrochemical electrodes.^{1,8-10}

The grains size, their misorientation and consequently the atomic structure of diamond grain boundaries plays a significant role on transport and mechanical properties.¹¹⁻¹⁵

Microcrystalline diamond CVD grown films usually exhibit highly textured laminar grains due to varying growth kinetics in different crystallographic directions. Both, grain sizes and texturing increase along the film cross-section. As a consequence, faster growing grains overgrow slower growing grains during film evolution.¹⁶ This phenomenon of evolutionary selection is often called Van der Drift growth mode¹⁷ and can be found in many crystalline materials, deposited by different methods.¹⁸ A schematic example of the resulting microstructure, developed by an evolutionary selective growth is shown in figure 1(a), next to figure 1(b), where the SEM image of the cross section of a microcrystalline diamond film is shown.

^aCorresponding author: Markus Mohr, markus.mohr@uni-ulm.de

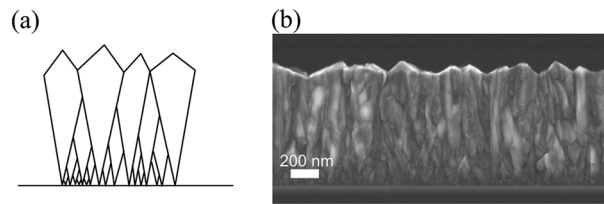


FIG. 1. (a) Schematic drawing of a thin film grown by the evolutionary selective growth mode after¹⁸ (b) SEM image showing the cross section of a microcrystalline diamond film.

Intriguing is the fact that the branched grain boundaries in figure 1(a) and (b) have similarities to the branches of the Stern-Brocot tree.^{19,20} Using the branching angle between the branched grain boundaries, a branching ratio r and subsequently the fractal dimension DH of the tree can be evaluated. Fractal analysis on the cross-section of microcrystalline diamond films are currently undertaken. A detailed analysis of the grains evolution during microcrystalline diamond growth will be subject of future work.

It is known that certain changes of growth parameters, such as an increase of the methane to hydrogen ratio decrease the average grain size down to the nanometer range.¹¹ This leads to smooth surfaces and hence consequently gives rise to the short run-in times needed for sliding nanocrystalline diamond bodies.⁹ Nonetheless, a very low grain size can also lead to reduced fracture strength of the (ultra-)nanocrystalline diamond films.³ That will make it necessary to find an optimum between smooth surface and fracture strength to obtain a wear resistant sliding contact.

However, in the present publication we are focusing on the fractal dimension of grain contours and on the surface fractal dimensions of microcrystalline diamond films.

As mentioned above, the average diameter of the grains measured in the film plane is increasing as a function of film thickness. The average grain diameter and its fractal geometry are important microstructural features, strongly influencing overall physical and chemical film properties (e.g. Refs. 21 and 22). For example, an important parameter for the thermal transport along the polycrystalline film (such as in the engineering application as a diamond heat-spreader) would be the average grain size perpendicular to the growth direction. Reaching a large average grain size perpendicular to the growth direction in short growth time would therefore be a goal to optimize such films morphology.

Also, mechanical properties, such as fracture stress and strain are directly influenced by the grain size and geometrical shape.²³ Often, grain boundaries and triple points are preferable locations for crack nucleation and growth, while at the same time, short periodicity and curved geometry of these boundaries can impede the growth of cracks²³ and thus improve fracture toughness.

The grains sizes and shapes of thin films, synthesized by vapor deposition methods, also influence their surface properties such as roughness and consequently frictional performance. The surface fractal dimensions of sliding surfaces have an important influence on the resulting friction force.²⁴

That way, the fractal dimension of grain interfaces can be used to develop more accurate models describing transport properties and mechanical properties of polycrystalline films. However, the limit of resolution in present days SEM equipment makes the presented approach difficult to apply for diamond films exhibiting grain sizes below about 100 nm.

In this work, we perform fractality analyses on grain contours, as well as on the surface morphology of diamond thin films, mainly based on scanning electron microscopy (SEM) images from Refs. 1 and 2.

Examples of fractal sets in mathematics and fractal objects in nature have been known throughout the century. The concept of fractal dimension was introduced by the early works of Mandelbrot.²⁵ Already in the work of Kaye,²⁶ simple correlations of particles fractal dimension and physical properties of the particles can be found. In the beginning 90ies, Mitic and Kocic improved the analysis of fractal dimensions, such that it enabled the application of fractal dimension analysis on microstructure of ceramics.^{27,28} That way, the Heywang model of intergranular capacities

was extended by correction factors taking into account the fractal dimension of the intergranular contacts.^{27,28}

Our common experience of dimensions is exhausted with the first three dimensions, 1 for a line, 2 for a surface and 3 for a volume. Eventually we may accept 0 as the dimension of a dot. This kind of dimension is called topological dimension,²⁹ denoted by DT . So, if $DT(S) = 1$, we are sure that the object S is a line, linear segment, piecewise linear curve or the limit of a sequence of piecewise linear curves, all in R^n . On the other hand, topological dimension is not applicable to fractal objects. For such objects, a generalization of the topological dimension, the non-dimensional number called Hausdorff dimension DH (also called ‘Hausdorff-Besicovitch dimension’ or just ‘fractal dimension’), is applicable. If $DH(S)$ is a non-integer, the set S is called fractal and the inequality $DH(S) > DT(S)$ holds.^{25,29,30}

In nature (and technology) it is, in contrary to mathematics, not easy to define a perfect rule for self-similarity. We rather speak of a statistical self-similarity.³⁰ The technological processes applied in thin film deposition lead to the deposition of molecule by molecule or even atom by atom onto the growth surface. This procedure causes the growth of layer over layer with repeating patterns and statistical self-similarity.

Hence, the objective of this paper is to apply procedures and methods developed in the study of sintered ceramics^{27,28,31–40} to thin film deposits and their morphology.

II. EXPERIMENTAL

Polycrystalline diamond films can be grown by different chemical vapor deposition (CVD) methods.^{41–44} The most versatile and scalable method is the hot filament chemical vapor deposition (HFCVD). Dependent on the grain sizes of the resulting film deposits, the films are usually categorized in microcrystalline diamond (MCD), nanocrystalline diamond (NCD) and ultrananocrystalline diamond (UNCD).⁴⁵ The temperature, total gas pressure and composition of gas mixture during deposition are essential growth parameters influencing the diamond layer’s morphology.⁴⁶

The diamond films were grown on perfectly polished 2” (100) single-crystal silicon substrates. Beforehand, ultrasonication inside a nanocrystalline diamond particle suspension was performed in order to achieve a high diamond nucleation density on the order of about 10^{11} cm^{-2} .^{3,8,9,47}

In the HFCVD chamber (CEMECON 800) the diamond films were deposited subsequently using a CH_4/H_2 gas mixture with varying the gas pressure at substrate temperatures of typically 700-750 °C for 8 hours for all samples.

In this work, we analyze the fractal dimension of the grain contours and film surface of a set of six micro-/nanocrystalline diamond thin films grown by HFCVD. While all other parameters were kept the same, only the gas pressure during growth was varied among the six samples.

SEM images of the sample surfaces were taken and used for the analysis of the films fractal nature. We applied various mathematical-physical methods (the Richardson plot, Power spectrum algorithm, Cube counting algorithm, Triangulation algorithm, Partitioning algorithm). In the following, we introduce the mathematical-physical methods that were applied on the SEM images:

A. Richardson plot and Kaye’s modification

The Richardson effect says that the perimeter length L of an area depends on the measurement scale δ : the smaller the measurement unit, the longer is the resulting perimeter. From the relation $L = \delta^{1-DH}$ where DH is fractal dimension of grain’s contour, we get a linear dependence

$$\log(L) = (1 - DH) \times \log(\delta) + C$$

in a log-log plot. The slope $A=1-DH$ can be used to obtain the fractal dimension of a grain’s contour using linear least-square approximation of the measurement data.

Brian Kaye divided the range of magnitude of the measurement unit roughly in three parts: Euclidean, textural and structural sub-ranges.^{26,48}

Euclidean sub-range. Below a value l_1 ($0 < l_1 < R$), all yardstick lengths l , $0 < l < l_1$, cannot “detect” anything but a straight line. This subinterval is called Euclidean, the fractal dimension in this interval tends to the topological dimension $DH \rightarrow DT$.

Textural sub-range. This sub range corresponds to the middle values of l , say $l_1 < l < l_2$, where the measurement compass constantly evidences the small, local unevenness; This subinterval is called textural subinterval.

Structural sub-range. This is the third part of the interval $(0, R)$, i.e., for $l_2 < l < R$, where the bigger details outweigh the smaller ones. This subinterval is called structural subinterval.

B. Power spectrum algorithm

The Herzfeld-Overbeck variant⁴⁹ of the power spectrum algorithm is based on the power spectrum dependence of fractional Brownian motion. In the power spectrum method,⁵⁰⁻⁵² every line height profile that forms the image is Fourier transformed and the power spectrum evaluated and then all these power spectra are averaged. Fractal dimension is evaluated from the slope β of a least-square regression line fit to the data points in log-log plot of power spectrum as $DH = 7/2 - \beta/2$.

$$H_{s,t} = \sum_{n=0}^{N-1} \sum_{m=0}^{N-1} f_{n,m} \exp\left[\frac{2\pi i}{N}(sn + tm)\right], \quad (s, t = 0, \dots, N-1)$$

the two-dimensional power spectral density is

$$W[f]_k = \frac{1}{\text{card}(I_k)} \sum_{(s,t) \in I_k} |H_{s,t}|^2, \quad I_k = \{(s,t) | k \leq r < k+1 \wedge r = \sqrt{s^2 + t^2}\}$$

and therefore, the set of points $(\log(k), \log(W[f]_k))$, $k=1, \dots, m$, where m is the maximum side length of a SEM sample picture (in pixels). The outcome is the slope coefficient of the linear least-square approximation through the set of points $(\log(k), \log(W[f]_k))$. This coefficient then participates in final evaluation of fractal dimension of the surface.

C. Cube counting algorithm

The algorithm^{53,54} is based on the following steps: a square lattice with distance ε is superimposed on the digital surface under consideration. The surface is scaled until it fits a unit square. In i -th step one sets $\varepsilon = i/2$. Then $N(\varepsilon)$ is the number of all squares that contain at least one pixel of the surface. The lattice constant l is then reduced stepwise by factor of 2 and the process repeated until ε equals to the distance between two adjacent pixels. The slope of a plot of $\log(N(\varepsilon))$ over $\log(1/\varepsilon)$ gives the fractal dimension DH .

D. Triangulation algorithm

The triangulation algorithm⁵³ is very similar to cube counting method and is also based directly on the box-counting fractal dimension definition. The method works as follows: a grid of unit dimension $\varepsilon = 1$ is placed on the surface. This defines the location of the vertices of a number of triangles. When, $\varepsilon = 1/2$, base of a surface is subdivided into 4 squares or in 8 triangles the surface is covered by 32 triangles of different areas inclined at various angles with respect to the xy plane. The areas of all triangles are calculated and summed to obtain an approximation of the surface area $S(l)$ corresponding to l . The grid size is then decreased by successive factor of 2, as before, and the process continues until l corresponds to distance between two adjacent pixel points. The slope of a plot of $(\log 1/\varepsilon, \log N(\varepsilon))$ then corresponds to $DH-2$.

E. Partitioning algorithm

Let $z = f(x, y)$ be an ideal fractal image with a 3D continuous surface.⁵⁵ It is divided into distinct copies and a copy has a minimum denoted as $z_1 = f(x_1, y_1)$ and a maximum denoted as $z_2 = f(x_2, y_2)$, when $x_1 < x_2$ and $y_1 < y_2$. Let dx and dy be the lengths of the copy in the directions of x and y , respectively, and dz be the height in the direction of z . Because $z = f(x, y)$ is continuous, we can obtain $dx = x_2 - x_1$, $dy = y_2 - y_1$, and $dz = z_2 - z_1$. Suppose $dx = dy$ and define the box scale as $r = dx = dy$. Assume a column of boxes with the size of $dx \times dx \times dx$ cover the copy of surface completely. The number of this column of boxes is equal to the integer part of $(dz/r + 1)$. Fractal dimension estimate of the ideal fractal surface can be calculated as

$$DH \sim -\frac{\log Nr_1 - \log Nr_2}{\log r_1 - \log r_2}$$

where Nr_1 and Nr_2 are the numbers of boxes covering the ideal fractal surface when the box scales are r_1 and r_2 , respectively. When r_1 and r_2 approach zero, the scale range can be found such that the DH estimate error approaches zero. Any two values of r in $[r_1, r_2]$ and their corresponding Nr can be used to obtain DH since Nr versus r is an exact straight line in a log–log plot in this scale range. The negative slope of the straight line is equal to DH .

III. RESULTS

In order to correlate growth conditions with the resulting unevenness of grain boundaries, we determined the fractal dimension of several grain contours. Furthermore, we calculated the surface fractal dimensions of several samples in order to correlate the surface morphology with growth conditions.

A. Grain contours fractal dimension

Here we first determine and analyze the fractal dimension DH of some of the grain's contours from SEM images of samples grown with a variation of gas pressure while the other growth parameters were kept the same. The images are shown in figure 2 (from Ref. 56).

In Fig. 3, we show the shape contour reconstruction and the associated fractal dimension diagrams, calculated by the method of Richardson and Kaye.

Figure 4 shows the average values of DH in the textural and structural sub-range as a function of growth-pressure. It can be observed that the different total gas pressures during the CVD growth influence both, the fractal dimension on a textural and on a structural sub-range.

B. Surface fractal dimension

Our first interest will be the estimation of quantitative measures for fractal dimensions of the top surface of the microcrystalline diamond thin films such as shown on SEM images (in perspective

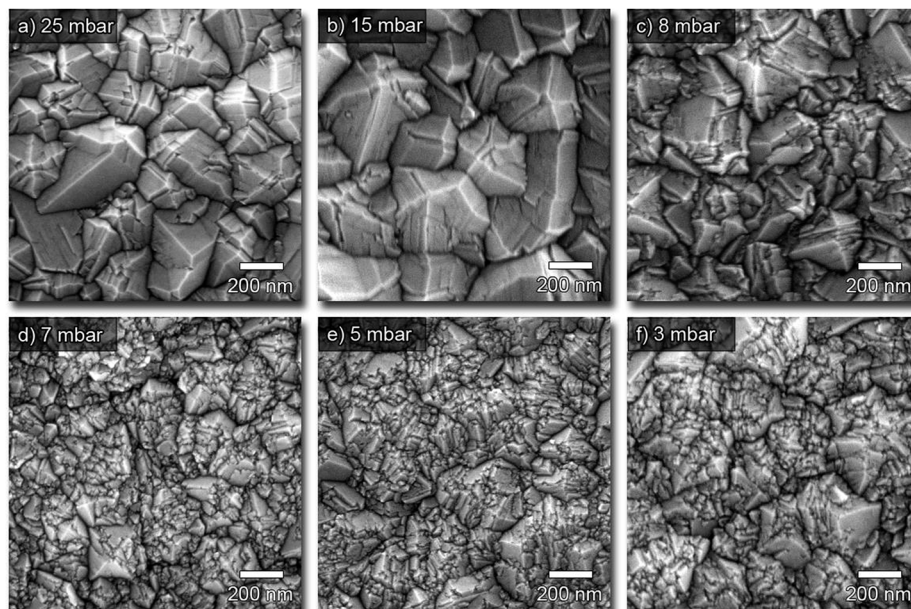


FIG. 2. SEM images taken from sample surfaces of six samples grown at different gas pressures. The influence of gas pressure on surface morphology and grain size can be seen. Reproduced with permission from M. Wiora, Characterization of nanocrystalline diamond coatings for micro-mechanical applications, PhD Thesis, University Ulm (2013). Copyright 2013 University Ulm.⁵⁶

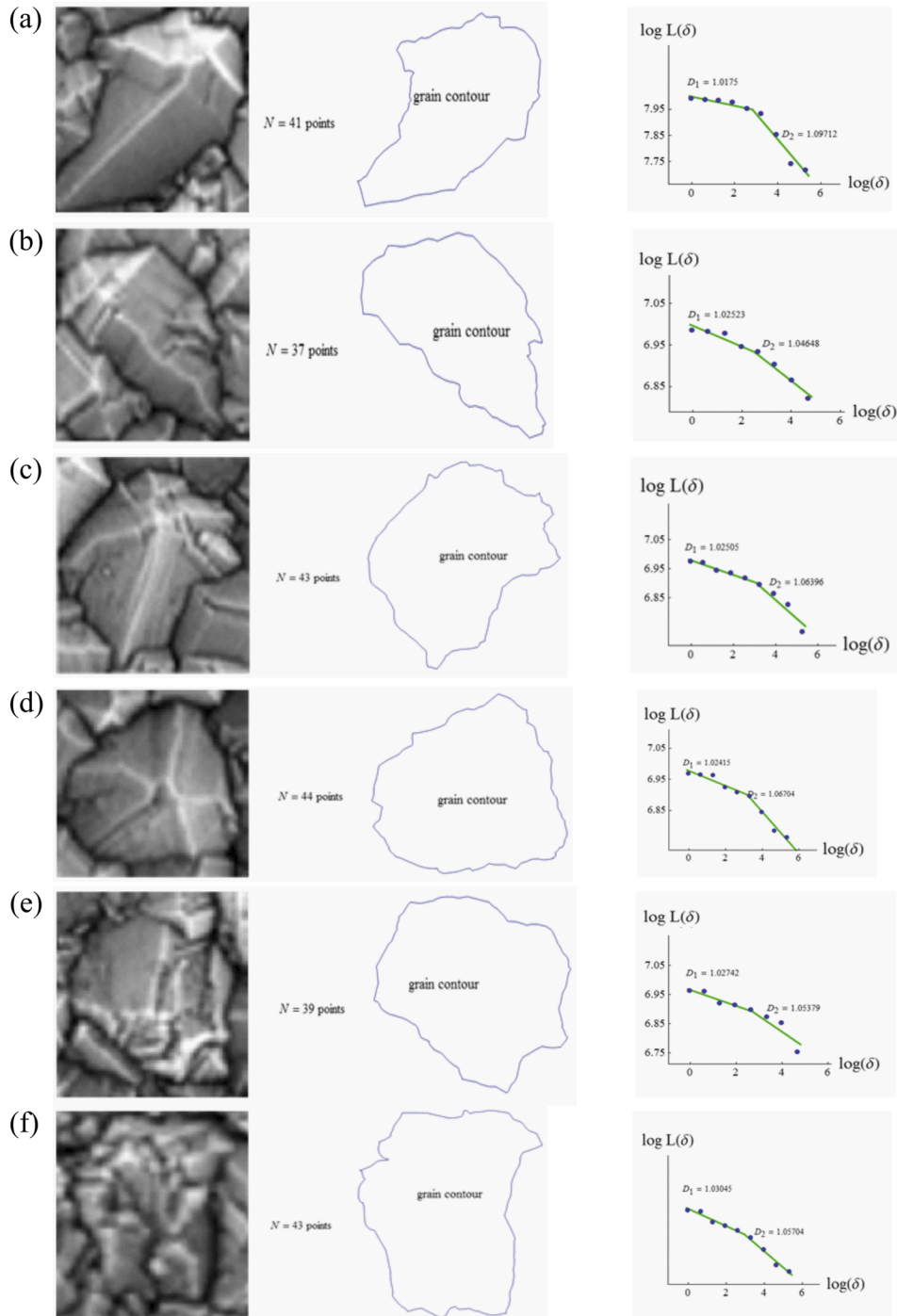


FIG. 3. Grain developed under different pressures; (a), (b) 25 mbar (c), (d) 15 mbar (e), (f) 8 mbar Richardson plot and Kaye's analysis presented.

projection) in Fig. 5(a) (from Ref. 56). Figure 6 shows the log-log-plots obtained by the partitioning method together with the obtained surface fractal dimensions for surfaces of diamond films grown at different pressures.

The diagram in Fig. 7 demonstrates the influence of different gas pressures during CVD growth on the resulting microstructure and directly on the surface fractal dimension. It is evident, that the fractal dimension, from 3 to 5 mbar total gas pressure approaches its local maximum; after that we

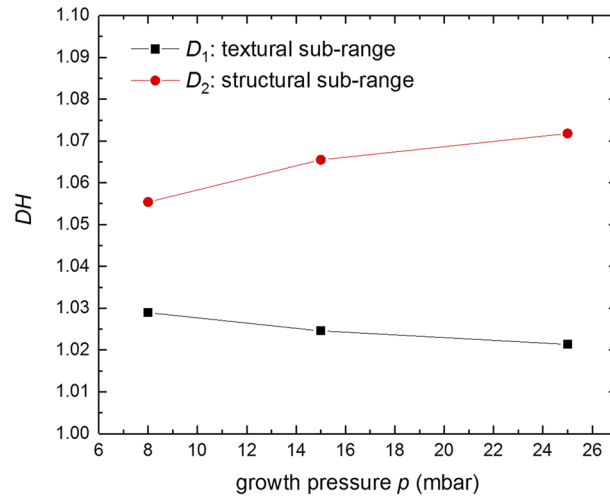


FIG. 4. Influence of gas pressure on the fractal dimensions of the grains contours.

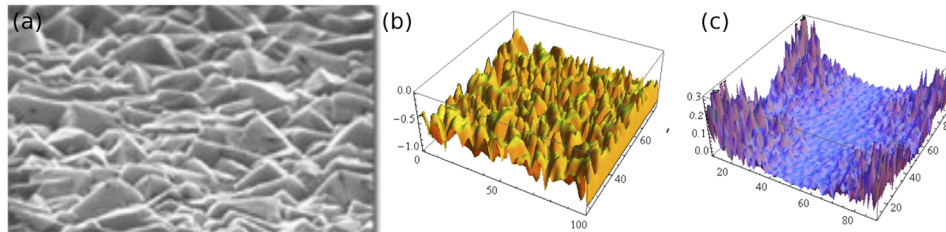


FIG. 5. (a) Surface of diamond film layer. Reproduced with permission from M. Wiora, Characterization of nanocrystalline diamond coatings for micro-mechanical applications, PhD Thesis, University Ulm (2013). Copyright 2013 University Ulm.⁵⁶ (b) Numerically generated surface of the left photo. (c) Discrete Fourier Transform (DFT) of the surface in the middle.

have up to 15 mbar decreasing fractal dimension and after that with pressure growing up to 25 mbar fractal dimension is slightly increasing.

IV. DISCUSSION

The grains contour fractal dimensions were found to be between about 1.02 and 1.07 for the investigated samples. In comparison to that, grains contour fractal dimension of ceramic materials prepared by sintering powder material were found to be between 1.1 and 1.3.³⁶ This shows that the investigated microcrystalline samples owing to their faceted grain surfaces have rather smooth grain contours, compared to sintered ceramics.

The grains contour fractal dimension is a measure of the interface roughness between grains and is hence influencing electrical and thermal transport between grains.^{21,22,57} As such, our results are important input parameters for the modeling of transport properties of microcrystalline diamond films.

The fractal dimension of the investigated CVD film surfaces was between 2.2 and 2.9, showing a much higher value than the fractal dimension of grains surfaces of sintered ceramics (2.01-2.02).³⁶ This is reasonable, considering the differences in the fabrication processes. The enhanced material transport processes during sintering will, by minimization of free energy, lead to ceramic grain shapes closer to a smooth equilibrium shape. In contrast to that, the CVD method takes place far away from thermodynamic equilibrium, not providing enough energy to drive considerable diffusion in the grown crystallites to perform shape changes. This leads to grain shapes, defined solely by the chemical deposition mechanism.

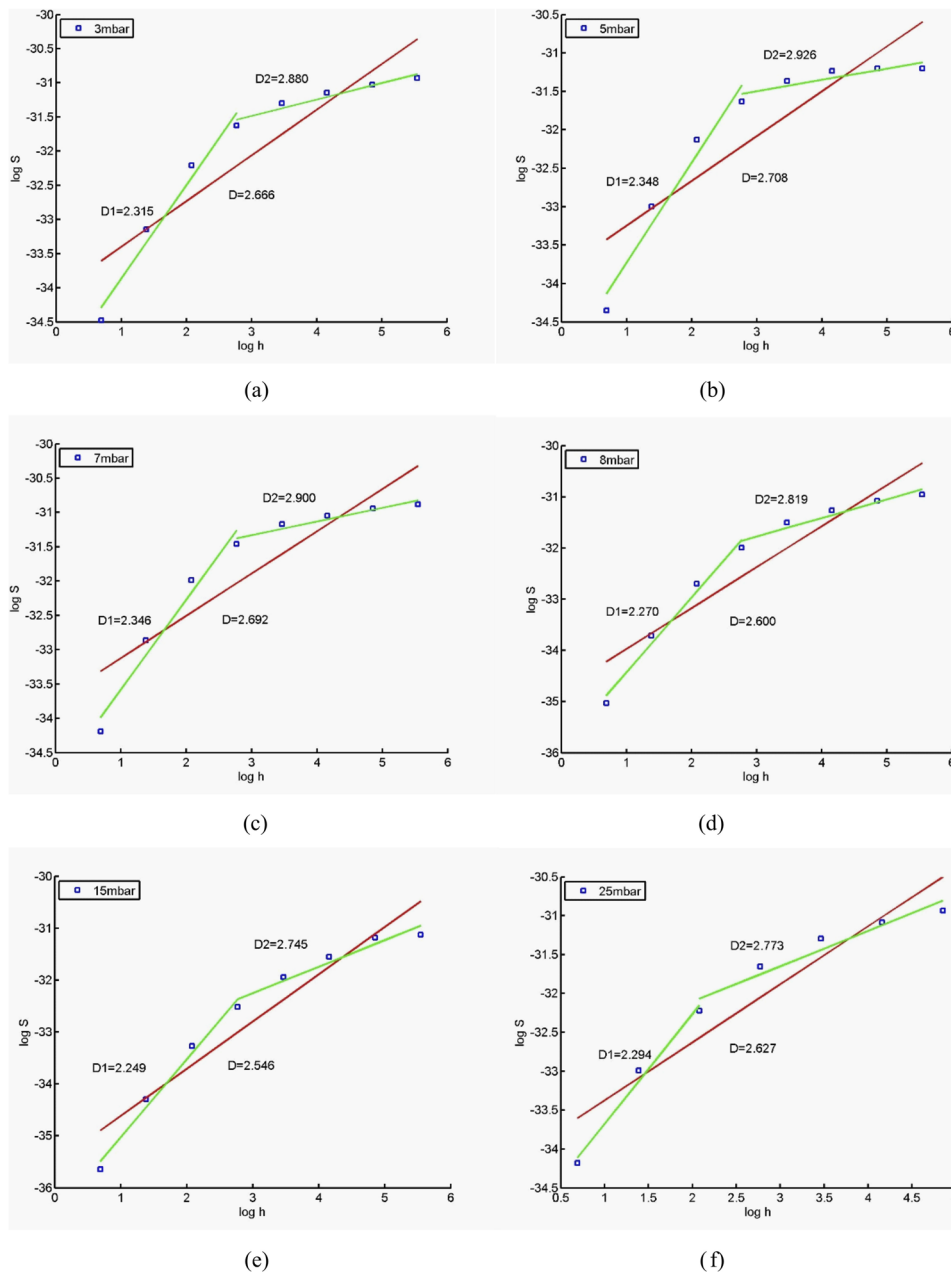


FIG. 6. Diamond film layers obtained under different pressures, estimation of its surface fractal dimensions by four different methods: log-log plots of the partitioning method are presented (a) 3 mbar (b) 5 mbar (c) 7 mbar (d) 8 mbar (e) 15 mbar (f) 25 mbar.

Models of the chemical reactions in the gas phase during CVD diamond growth come to the conclusion, that grain size is mainly determined by the ratio of atomic hydrogen to hydrocarbon radicals at the growth surface (H/CH_x) and in addition varies by the substrate temperature.^{46,58} In the used HFCVD setup, both depends on the used growth pressure. The substrate temperature is indirectly set by the filament temperature and the thermal transport in the gas phase, which is increasing with increasing gas pressure.⁵⁹ According to,⁵⁸ the expected growth rate of CVD diamond is increasing with increasing concentration of atomic hydrogen until it saturates for even higher atomic hydrogen concentrations. The rate of defect generation, leading possibly to the nucleation of new grains, is however proportional to the growth rate and inversely proportional to the square of the concentration

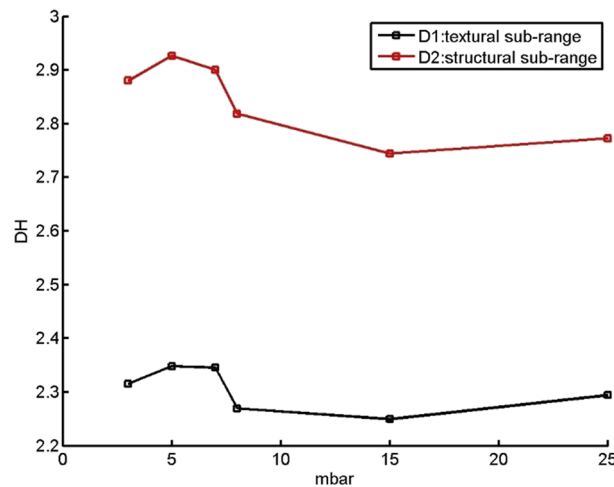


FIG. 7. Influence of growth gas pressures on microstructure and on the surface fractal dimension DH .

of atomic hydrogen.⁵⁸ That way, an increasing growth rate can be expected for an increasing H/CH_x ratio, together with a decreasing defect generation rate.^{46,58} A higher amount of atomic hydrogen on the growth surface leads to the suppression of growth defects and enables migration of hydrocarbon on the growth surface to attach to step-edges, forming faceted crystallites.⁴⁶

We can understand the grains contour fractal dimension changes in the structural sub-range (Fig. 4) as the influence of gas pressure on the thin film formation. At first, we can see that fractal dimension in the structural sub-range is higher than the fractal dimension in the textural sub-range. It is evident, that a higher gas pressure during growth results in a slight increase of grains contour fractal dimension in the structural sub-range. At the same time, a slight decrease of fractal dimension in the textural sub-range takes place with increasing gas pressure.

This can be understood by a higher ratio of H/CH_x forming on the substrate for higher pressures. This leads to the formation of bigger grains with clear facets, which gets obvious by rougher contours on a large length scale (textural sub-range), while smoother grain contours on a smaller length scale (structural sub-range) occur for higher pressure.

Regarding the development of the grains surface fractal dimension with pressure (Fig. 7), the gas pressure has the same effect on the fractal dimension in both, structural and textural sub-ranges. Again, the fractal dimension value for the structural sub-range is higher than for the textural sub-range. As can be seen in Fig. 7, for small gas pressures, the surface fractal dimensions increase with increasing gas pressures and are approaching a maximum for gas pressure values around 5 mbar. This is explainable by an increase of atomic hydrogen, produced on the filaments with increasing pressure,⁶⁰ hence leading to an increasing growth rate and due to the still large defect generation and renucleation rate to an increasingly rough surface with higher fractal dimensions. For increasing pressure, the fractal dimensions decrease. This is explained by the higher atomic hydrogen to hydrocarbon ratio on the growth surface, together with a higher substrate temperature. This leads to less growth defects, lower renucleation rate and better surface migration of the growth species, leading to the formation of smooth crystalline facets.

The visual inspection of the film morphologies in figure 1 gives certainly the same, qualitative impression. However, the fractal dimension analysis offers a metric for the quantitative characterization of the surface morphology of CVD diamond thin films and as such, gives a quantitative description.

This can be used for models, describing friction coefficients of sliding interfaces¹⁸ or transport properties.

Both, the grains contour fractal dimension as well as the surface fractal dimension can be used as input parameters for models predicting diamond thin films properties. As such, the determination of CVD diamonds grains contour fractal dimension and surface fractal dimension can be used as parameters guiding the tailoring of film properties to the demands of the desired application.

V. CONCLUSION

In this work, the fractal nature analysis developed for ceramics materials was applied to micro- and nanocrystalline diamond thin films. That way, we compared the fractal dimension to the surface morphology obtained at different growth pressures. The total gas pressure during diamond film growth has influence on the films microstructure and morphology. The contour and surface fractal dimensions complementarity, form a metric that can be used to describe the films surface morphology. Film morphologies with large faceted grains show low surface fractal dimensions, while films with small grains possess a higher surface fractal dimension. We described the relation between growth conditions, the surface morphology and the fractal dimensions. This way, a new way of surface characterization is presented, which gives more insights into the sample morphology than a simple roughness measurement of the sample could give.

The potential of the fractal dimension as a characteristic for grains contours or grains surfaces will be used in future modeling work to connect the grain size and shape to physical properties of the CVD grown diamond thin films.

- ¹ S. O. Kucheyev, J. Biener, J. W. Tringe, Y. M. Wang, P. B. Mirkarimi, T. van Buuren, S. L. Baker, A. V. Hamza, K. Brühne, and H.-J. Fecht, *Appl. Phys. Lett.* **86**, 221914 (2005).
- ² M. Wiora, K. Brühne, and H.-J. Fecht, Synthesis of Nanodiamond, in: H.-J. Fecht, K. Brühne, and P. Gluche (eds.), *Carbon-Based Nanomaterials and Hybrids, Synthesis, Properties, and Commercial Applications*, Pan Stanford Publ. Pte. Ltd. (2014), 5–48.
- ³ M. Mohr, A. Caron, P. Herbeck-Engel, R. Bennewitz, P. Gluche, K. Brühne, and H.-J. Fecht, *Journal of Applied Physics* **116**, 124308 (2014).
- ⁴ S. Bhattacharyya, O. Auciello, J. Birrell, J. A. Carlisle, L. A. Curtiss, A. N. Goyette, D. M. Gruen, A. R. Krauss, J. Schlueter, A. Sumant, and P. Zapol, *Applied Physics Letters* **79**, 1441 (2001).
- ⁵ M. Mertens, M. Mohr, N. Wiora, K. Brühne, and H.-J. Fecht, *Journal of Nanomaterials* 527025 (2015).
- ⁶ N. Wiora, M. Mertens, K. Brühne, H.-J. Fecht, I. C. Tran, M. T. Willey, A. van Buuren, J. Biener, and J.-S. Lee, *Journal of Applied Physics* **122**, 145102 (2017).
- ⁷ N. Wiora, M. Mertens, M. Mohr, K. Brühne, and H.-J. Fecht, *Diamond and Related Materials* (2016), **70**, p. 145.
- ⁸ M. Mohr, A. Behroudj, N. Wiora, M. Mertens, K. Brühne, and H.-J. Fecht, *Quantum Matter* **6**, 41 (2017).
- ⁹ M. Mohr, M. Mertens, K. Brühne, P. Gluche, and H.-J. Fecht, *Keramische Zeitschrift* **69**, 115 (2017).
- ¹⁰ M. Wiora, R. Gretzschel, S. Strobel, and P. Gluche, Industrial Applications and Commercial Perspectives of Nanocrystalline Diamond, in: H.-J. Fecht, K. Brühne, and P. Gluche (Eds.), *Carbon-Based Nanomaterials and Hybrids – Synthesis, Properties, and Commercial Applications*, Pan Stanford (2014), ISBN: 978-981-4316-85-9.
- ¹¹ M. Mohr, L. Daccache, S. Horvat, K. Brühne, T. Jacob, and H.-J. Fecht, *Acta Materialia* **122**, 92 (2017).
- ¹² J. Anaya, S. Rossi, M. Alomari, E. Kohn, L. Tóth, B. Pécz, K. D. Horbart, T. J. Anderson, T. I. Feygelson, B. B. Pate, and M. Kuball, *Acta Materialia* **103**, 141 (2016).
- ¹³ D. Spiteri, J. Anaya, and M. Kuball, *Journal of Applied Physics* **119**, 085102 (2016).
- ¹⁴ W. Lojkowski and H.-J. Fecht, *Progress in Materials Science* **45**, 339 (2000).
- ¹⁵ K. Tai, A. Lawrence, M. P. Harmer, and S. J. Dillon, *Applied Physics Letters* **102**, 034101 (2013).
- ¹⁶ A. van der Drift, *Philips Res. Rep.* **22**, 267–288 (1967).
- ¹⁷ C. Wild, *J. Appl. Physics* **68**, 973–978 (1990).
- ¹⁸ J. E. Yehoda and R. Messier, *Applications of Surface Science* **22/23**, 590–595 (1985).
- ¹⁹ A. Brocot, *Revue Chronométrique* **3**, 186–194 (1861).
- ²⁰ M. A. Stern, *Journal für die reine und Angewandte Mathematik* **55**, 193–220 (1858).
- ²¹ S. B. Soffer, *Journal of Applied Physics* **38**, 1710 (1967).
- ²² A. F. Mayadas and M. Shatzkes, *Physical Review B* **1**, 1382 (1969).
- ²³ I. A. Ovid'ko, *Phil. Trans. R. Soc. A* **373**, 20140129 (2015).
- ²⁴ W. Pan, X. Li, L. Wang, J. Mu, and Z. Yang, *AIP Advances* **7**, 095321 (2017).
- ²⁵ B. Mandelbrot, *The Fractal Geometry of Nature* (W. H. Freeman and Co., New York, 1982).
- ²⁶ B. K. Kaye, *A Random Walk Through Fractal Dimensions* (VCH Publishers, New York, 1989).
- ²⁷ V. V. Mitic, Lj. M. Kocic, and I. Z. Mitrovic, Fractals in Ceramic Structure, Proc. of the IX World Round Table Conference on Sintering held in Belgrade from 1-4. September 1998: Advanced Science and Technology of Sintering, edited by Stojanovic et al., Kluwer Academic/Plenum Publishers, New York (1999), 397–402.
- ²⁸ V. V. Mitic, Lj. M. Kocic, and I. Z. Mitrovic, Fractals and BaTiO₃-Ceramics Intergranular Impedance, Gordon Research Conference: Ceramics, Solid State Studies in Ceramics, Kimball Union Academy, Meriden, New Hampshire, August 1–6 (1999).
- ²⁹ M. Barnsley, *Fractals Everywhere* (Academic Press, San Diego, 1988).
- ³⁰ H.-O. Peitgen, H. Juergens, and D. Saupe, *Chaos and fractals*, 2ed. (Springer, 2004).
- ³¹ V. V. Mitic, Lj. M. Kocic, I. Z. Mitrovic, and M. M. Ristic, Shapes and Grains Structures Stochastic Modelling in Ceramics, Proc. of S4G - International Conference on Stereology, Spatial Statistics and Stochastic Geometry, Prague, Czech Republic, June 21–24, 209 (1999).
- ³² V. Mitic, V. B. Pavlovic, Lj. Kocic, V. Paunovic, and D. Mancic, Application of intergranular and fractal impedance model on optimisation of BaTiO₃ properties, 33rd International conference and exposition on Advanced ceramics and composites, Daytona Beach **14** (2009).

- ³³ V. Mitic, V. Pavlovic, Lj. Kocic, V. Paunovic, and Lj. Živkovic, *CIMTEC* **93** (2010).
- ³⁴ V. Mitic, V. B. Pavlovic, Lj. Kocic, V. Paunovic, M. Miljkovic, and Lj. Živkovic, *Electronic Materials and Applications* **43** (2010).
- ³⁵ V. V. Mitic, V. Paunovic, and Lj. Kocic, Dielectric Properties of BaTiO₃ Ceramics and Curie-Weiss and Modified Curie-Weiss Affected by Fractal Morphology, in: *Advanced Processing and Manufacturing Technologies for Nanostructured and Multifunctional Materials* (T. Ohji, M. Singh, and S. Mathur eds.), *Ceramic Engineering and Science Proceedings* **35**, 123 (2014).
- ³⁶ V. V. Mitic, Lj. Kocic, V. Paunovic, and V. Pavlovic, *Science of Sintering* **46**, 149 (2014).
- ³⁷ V. V. Mitic, V. Paunovic, and Lj. Kocic, *Ceramics Int.* **41**, 6566 (2015).
- ³⁸ V. V. Mitic, Lj. Kocic, V. Paunovic, F. Bastic, and D. Sirmic, *Sci. of Sintering* (2015).
- ³⁹ P. Petkovic, V. V. Mitic, and Lj. Kocic, *Folia Anatomica* **26**, 67 (1998).
- ⁴⁰ A. Terzic, Z. Radojevic, M. Arsenovic, V. V. Mitic, S. Pasalic, and Lj. Kocic, *39th Int'l Conf & Expo on Advanced Ceramics & Composites ICACC* (2015).
- ⁴¹ E. Sevillano, *Low-Pressure Synthetic Diamond, Springer Berlin Heidelberg*, (1998) Chapter 2: Microwave-Plasma Deposition of Diamond, page 11–39.
- ⁴² C. A. Wolden, *Diamond Films Handbook*, Marcel Dekker, Inc. (2002), Chapter 8: Combustion Synthesis of Diamond, page 303.
- ⁴³ S. Matsumoto, Y. Sato, M. Kamo, and N. Setaka, *Journal of Materials Science* **17**, 3106 (1982).
- ⁴⁴ S. Matsumoto, Y. Sato, M. Kamo, and N. Setaka, *Japanese Journal of Applied Physics Part 2* **21**, 183 (1982).
- ⁴⁵ O. A. Williams, M. Nesladek, M. Daenen, S. Michaelson, A. Hoffman, E. Osawa, K. Haenen, and R. B. Jackman, *Diamond and Related Materials* **17**, 1080 (2008).
- ⁴⁶ P. W. May and Y. A. Mankelevich, *J. Phys. Chem. C.* **112**, 12432 (2008).
- ⁴⁷ M. Mertens, I.-N. Lin, D. Manoharan, A. Moheiniyan, K. Brühne, and H.-J. Fecht, *AIP Advances* **7**, 015312 (2017).
- ⁴⁸ B. H. Kaye, *Powder Technology* **21**, 1 (1978).
- ⁴⁹ U. C. Herzfeld and C. Overbeck, *Comp & Geosciences* **25**, 979 (1999).
- ⁵⁰ A. Van Put, A. Vertes, D. Wegrzynek, B. Treiger, and R. Van Grieken, *Fresenius J Anal Chem* **350**, 440 (1994).
- ⁵¹ A. Mannelquist, N. Almquist, and S. Fredriksson, *Appl. Phys. A* **66**, 891 (1998).
- ⁵² W. Zahn and A. Zösch, *Fresenius J Anal Chem* **358**, 119 (1997).
- ⁵³ C. Douketis, Z. Wang, T. L. Haslett, and M. Moskovits, *Physical Review B* **51**, 11022 (1995).
- ⁵⁴ W. Zahn and A. Zösch, *Fresenius J Anal Chem* **365**, 168 (1999).
- ⁵⁵ J. Li, Q. Du, and C. Sun, *Pattern Recognition* **42**, 2460 (2009).
- ⁵⁶ M. Wiora, Characterization of nanocrystalline diamond coatings for micro-mechanical applications, PhD Thesis, University Ulm (2013).
- ⁵⁷ D. Aurongzeb, M. Holtz, J. M. Berg, A. Chandolu, and H. Temkin, *Journal of Applied Physics* **98**, 063708 (2005).
- ⁵⁸ D. G. Goodwin, *Journal of Applied Physics* **74**, 6888 (1993).
- ⁵⁹ S. J. Harris and A. M. Weiner, *Journal of Applied Physics* **75**, 5026 (1994).
- ⁶⁰ S. Schwarz, S. M. Rosiwal, M. Frank, D. Breidt, and R. F. Singer, *Diamond and Related Materials* **11**, 589 (2002).